Blind Rigid Motion Estimation for Arbitrary MRI Sampling Trajectories

Anita Möller[1], Marco Maass[1], Tim J. Parbs[1], Alfred Mertins[1]

[1]Institute for Signal Processing, Universität zu Lübeck
moeller@isip.uni-luebeck.de

Abstract. In this publication, a new blind motion correction algorithm for magnetic resonance imaging for arbitrary sampling trajectories is presented. Patient motion during partial measurements is estimated. Exploiting the image design, a sparse approximation of the reconstructed image is calculated with the alternating direction method of multipliers. The approximation is used with gradient descent methods with derivatives of a rigid motion model to estimate the motion and extract it from the measured data. Adapted gridding is performed in the end to receive reconstruction images without motion artifacts.

1 Introduction

Artifacts caused by patient motion result in diagnostically unusable images measured by magnetic resonance imaging (MRI). These artifacts appear especially as ghost replications of the object or image blurring. In many cases, motion can be avoided by a motionless patient. But especially the motion of organs like lung, liver, and heart can not be stopped for a long time and also swallowing can not be suppressed effectively. To overcome these artifacts, techniques are developed to either adapt the measurement process to the motion or compensate motion afterwards.

In contrast to other method, blind motion estimation uses only information about the motion hidden in the measurement. The main idea is not to restrict oneself to periodical motion but also be capable of compensating spontaneous motion. Based on the knowledge about the sampling trajectories many methods were developed to estimate the performed motion. Then, it is extracted from the measurement data to reconstruct images without artifacts. One popular technique was proposed for rotated blade sequences by Pipe et al. [1] and is implemented in current MR scanners. There, motion is estimated from several partial measurements based on their correlation.

Former research showed that MR images can effectively be represented in sparse domains. Sparsification reduces the artifacts appearing in those representations. This was used to blindly estimate motion in [2]. The new proposed algorithm measures the MRI k-space on arbitrary trajectories and combines the ideas of sparsifying images and gradient descent algorithms. This leads to an image reconstruction algorithm with very high reduction of motion artifacts.

2 Materials and methods

In MRI, as the k-space contains sampled frequency coefficients, it can be interpreted as Fourier transform of the MR image. More exactly, one measurement of the whole k-space is composed of partial measurements at intervals in time specified by trajectories. Let $\boldsymbol{x}(\boldsymbol{r}) \in \mathbb{R}^{o \times m}$ be a two dimensional MR image with spatial coordinates $\boldsymbol{r} = [\boldsymbol{r}_1, \boldsymbol{r}_2, \ldots, \boldsymbol{r}_M] \in \mathbb{R}^{2 \times M}, M = om$ and $\boldsymbol{r}_i = [r_{i,1}, r_{i,2}]^T, i \in \{1, 2, \ldots, M\}$ with coordinate ranges $r_{i,1} \in [0, o-1], r_{i,2} \in [0, m-1]$

The Fourier transform of the image is described by $\mathcal{F}\boldsymbol{x}$. Parts of the k-space are sampled in consecutive time intervals indexed by $n = 1, 2, \ldots, N \in \mathbb{N}$ The read out is so fast that no motion occurs during these intervals. Let $\mathcal{S}(\boldsymbol{k}_n)$ be a sampling operator at frequency coordinates $\boldsymbol{k}_n$ belonging to all trajectory points measured at time n. The frequency coordinates of the samples are defined by $\boldsymbol{k}_n = [\boldsymbol{k}_{n,1}, \boldsymbol{k}_{n,2}, \ldots, \boldsymbol{k}_{n,P_n}] \in \mathbb{R}^{2 \times P_n}$ with two-dimensional coordinates $\boldsymbol{k}_{n,q} = [k_{n,q,1}, k_{n,q,2}]^T, q \in \{1, 2, \ldots, P_n\}$ in the ranges $k_{n,q,1} \in \left[-\frac{o-1}{2}, \frac{o-1}{2}\right], k_{n,q,2} \in \left[-\frac{m-1}{2}, \frac{m-1}{2}\right]$ With it, the partial measurement $\boldsymbol{y}_n(\boldsymbol{k_n}) \in \mathbb{C}^{P_n}$ with $P_n \in \mathbb{N}$ being the number of samples measured at this time n is given by $\boldsymbol{y}_n(\boldsymbol{k}_n) = \mathcal{S}(\boldsymbol{k}_n)\mathcal{F}\boldsymbol{x}$

If patients move during a complete MR scan, the partial measurements represent a motion corrupted image each. This motion is modeled by the operator $\mathcal{T}_{\boldsymbol{\theta}_n}$, where $\boldsymbol{\theta}_n \in \mathbb{R}^{\Theta}, \Theta \in \mathbb{N}$ contains all motion parameters necessary to describe the object motion from the first measurement at $n = 1$ to time n. In total, the partial measurement model is given by $\boldsymbol{y}_n(\boldsymbol{k}_n) = S(\boldsymbol{k}_n)\mathcal{F}\mathcal{T}_{\boldsymbol{\theta}_n}\boldsymbol{x}$ and the complete measurement is $\boldsymbol{y}(\boldsymbol{k}) = [\boldsymbol{y}_1(\boldsymbol{k}_1), \boldsymbol{y}_2(\boldsymbol{k}_2), \ldots, \boldsymbol{y}_N(\boldsymbol{k}_N)]$ with $\boldsymbol{k} = [\boldsymbol{k}_1, \boldsymbol{k}_2, \ldots, \boldsymbol{k}_N]$ Then, the reconstruction problem for the measured image $\hat{\boldsymbol{x}} \in \mathbb{R}^{o \times m}$ from all partial measurements $\boldsymbol{y}_n(\boldsymbol{k})_n$ can be formulated as

$$\hat{\boldsymbol{x}} = \arg\min_{\boldsymbol{x}} \sum_{n=1}^{N} \|\mathcal{S}(\boldsymbol{k}_n)\mathcal{F}\mathcal{T}_{\boldsymbol{\theta}_n}\boldsymbol{x} - \boldsymbol{y}_n(\boldsymbol{k}_n)\|_2^2 + \frac{1}{\sigma^2}\Phi(\boldsymbol{x}) \tag{1}$$

with a regularization term $\Phi(\boldsymbol{x})$ and $0 < \sigma \in \mathbb{R}$.

2.1 Rigid motion model

To model patient motion, we restrict ourselves to rigid motion. Therefore, we need three motion parameters $\boldsymbol{\theta}_n = [\beta_{n,1}, \beta_{n,2}, \alpha_n]$ in two dimensions. The translation operator is given by $\mathcal{D}_{\theta_{n,1},\theta_{n,2}}$ and the rotation is described by $\mathcal{R}_{\alpha_n}$. Then, the complete motion operator is given by $\mathcal{T}_{\boldsymbol{\theta}_n}\boldsymbol{x} = \mathcal{D}_{\beta_{n,1},\beta_{n,2}}\mathcal{R}_{\alpha_n}\boldsymbol{x}$

Translationmodel From [2], for a shift $\beta_{n,i} = \delta_{n,i} + \gamma_{n,i}$ with $\delta_{n,i} \in \mathbb{N}, \gamma \in (0, 1], i \in \{1, 2\}$, it is known that the translation transform is given by

$$\mathcal{D}_{\beta_{n,1},\beta_{n,2}}\boldsymbol{x} = D_{\gamma_{n,1}} D_1^{\delta_{n,1}} \boldsymbol{x} \left(D_1^{\delta_{n,2}}\right)^T D_{\gamma_{n,2}}^T \tag{2}$$

with convolution matrices $D_{\gamma_{n,i}}$ realising subpixel shift and D_1 realising full pixel circular shifts of the image.

Rotation model The rotation of the image is described with a rotation matrix $R_{\alpha_n} \in \mathbb{R}^{2\times 2}$ which rotates the coordinates $\boldsymbol{r}$ of the image $\boldsymbol{x}$. Afterwards, the image is interpolated back onto the unrotated coordinates by barycentric interpolation $I(\boldsymbol{x}(R_{\alpha_n}\boldsymbol{r}), \boldsymbol{r})$ [3] combined with Delaunay triangulation [4], to cope with arbitrary spatial grids. In total, the rotation model is described by

$$\mathcal{R}_{\alpha_n}\boldsymbol{x} = I(\boldsymbol{x}(R_{\alpha_n}\boldsymbol{r}), \boldsymbol{r}) \tag{3}$$

2.2 Nonequidistant sampling scheme

To allow for any arbitrary sampling trajectory, the operator $\mathcal{S}$ is able to sample any point $\boldsymbol{k}_{n,q} \in \mathbb{R}^{2\times 1}$ in frequency domain. This sampling can be formulated as nonequidistant discrete Fourier transform (NDFT) [5]

$$\boldsymbol{y}_n(\boldsymbol{k}_{n,q}) = \mathcal{S}(\boldsymbol{k}_{n,q})\mathcal{F}\boldsymbol{x}(\boldsymbol{r}) = \sum_{i=1}^{M} \boldsymbol{x}(\boldsymbol{r}_i) e^{-2\pi j \boldsymbol{k}_{n,q}^T \boldsymbol{r}_i},\ q = 1, 2, \ldots, P_n \tag{4}$$

2.3 Regularization

Generally, MR images consist of clear structures and edges and should not show noise. Especially, motion artifacts like ghosting appear as noise. So, the reconstructed images are supposed to be sparse in the wavelet domain. Therefore, the regularization term is chosen as $\Phi(\boldsymbol{x}) = \|\mathcal{W}\boldsymbol{x}\|_1$ with $\mathcal{W}$ being the wavelet transform. In the proposed setup, especially Daubechies wavelets are efficient.

2.4 Motion estimation gradient

Motion estimation is performed in a three-step iterative algorithm. It is based on the assumption that MR images can be sparsely represented in the wavelet domain. For each partial measurement n, separate motion parameters $\hat{\boldsymbol{\theta}}_n$ are estimated. The following algorithmic steps are iterated for each partial measurement separately.

Sparsifying by alternating direction method of multipliers (ADMM) The ADMM [6] solves (1) for fixed motion parameters $\hat{\boldsymbol{\theta}}_n$. It converges to the sparsest image $\hat{\boldsymbol{x}}$ representing partial measurements $\boldsymbol{y}_{n\in\Upsilon}$ whereby Υ contains all indexes n for measurements $\boldsymbol{y}_n$ with already estimated $\hat{\boldsymbol{\theta}}_n$ and the index of the currently considered measurement.

Problem (1) is split into two separate minimization problems and is iteratively updated by

$$\hat{\boldsymbol{x}}_{d+1} = \arg\min_{\boldsymbol{x}} \sum_{n\in\Upsilon} \|\mathcal{S}(\boldsymbol{k}_n)\mathcal{F}\mathcal{T}_{\hat{\boldsymbol{\theta}}_n}\boldsymbol{x} - \boldsymbol{y}_n(\boldsymbol{k}_n)\|_2^2 + \frac{1}{\lambda^2}\|\boldsymbol{x} - \bar{\boldsymbol{x}}_{d+1}\|_2^2$$

$$\bar{\boldsymbol{x}}_{d+1} = \hat{\boldsymbol{v}}_d - \boldsymbol{u}_d \tag{5}$$

$$\hat{\boldsymbol{v}}_{d+1} = \arg\min_{\boldsymbol{v}} \|\mathcal{W}\boldsymbol{v}\|_1 + \frac{\sigma^2}{\lambda^2}\|\boldsymbol{v} - \bar{\boldsymbol{v}}_{d+1}\|_2^2, \quad \bar{\boldsymbol{v}}_{d+1} = \hat{\boldsymbol{x}}_{d+1} + \boldsymbol{u}_d \tag{6}$$

$$\boldsymbol{u}_{d+1} = \boldsymbol{u}_d + \hat{\boldsymbol{x}}_{d+1} - \hat{\boldsymbol{v}}_{d+1} \tag{7}$$

with $\lambda, \sigma \in \mathbb{R}$, $\boldsymbol{u}_d, \boldsymbol{v}_d \in \mathbb{R}^{o \times m}$ and iteration index $d \in \mathbb{N}$. The measurement fitting problem (5) is solved by a conjugate gradient method [7] using the inverse NDFT (INDFT) [6]. The sparsifying step (6) is performed by soft thresholding.

Motion estimation by quasi-Newton gradient descent Gradients of the motion models (2), (3) with respect to $\beta_{n,1}, \beta_{n,2}$, and α_n are optimized in a quasi-Newton gradient descent with backtracking line search to estimate the motion. The Boyden, Fletcher, Goldfarb, and Shanno update rule [7] is used. The translation gradient is additionally parameterized by convolution with a Gaussian model.

Three gradient descents are calculated on the sparse image $\hat{\boldsymbol{x}}$ until an update for $\hat{\boldsymbol{\theta}}_{n,A_n}$ with $A_n \in \mathbb{N}$ being the iteration number per partial measurement is given. First, the rotation gradient is evaluated to get a first estimation for $\hat{\alpha}_{n,a}, a = 1, 2, \ldots, A_n \in \mathbb{N}$ With a sparse image temporarily rotated by $\hat{\alpha}_{n,a}$, the translation estimation gradient is applied in the quasi-Newton manner for both directions $\hat{\beta}^a_{n,1}, \hat{\beta}^a_{n,2}$ Finally, starting from the former estimations, all three motion parameters are estimated in one gradient for rotation and translation.

Motion update The estimated motion is added to a global motion $\hat{\boldsymbol{\theta}}_n = \hat{\boldsymbol{\theta}}_{n,A_n} = \sum_{a=1}^{A_n} \hat{\boldsymbol{\theta}}_{n,a}$ The sampling trajectory coordinates per partial measurement are updated by rotation with $\hat{\alpha}_{n,A_n}$, and image translation $[\hat{\beta}_{n,1,A_n}, \hat{\beta}_{n,2,A_n}]$ is updated in its frequency coefficients by phase shifts.

2.5 Image reconstruction

Finally, the global translation $[\hat{\beta}_{n,1}, \hat{\beta}_{n,2}]$ per partial measurement n is corrected by a phase shift in k-space. Afterwards, the global rotation per partial measurement is compensated by rotating the frequency coordinates by the estimated angle $\hat{\alpha}_n$ with $\hat{\boldsymbol{k}}_n = R_{\hat{\alpha}_n} \boldsymbol{k_n}$ In total, we get translation corrected frequency coefficients $\hat{\boldsymbol{y}}_n(\hat{\boldsymbol{k}}_n)$ which belong to rotated sampling coordinates in k-space.

The final reconstruction is done by gridding to avoid blurring caused by the INDFT. We follow the gridding scheme of Pipe et al. [8]. With it, the reconstruction is described by

$$\tilde{\boldsymbol{y}}\left(\boldsymbol{k}_g\right) = \left(\left(\left(\hat{\boldsymbol{y}}\left(\hat{\boldsymbol{k}}\right) w_\omega\left(\hat{\boldsymbol{k}}\right)\right) * c\left(\hat{\boldsymbol{k}}\right)\right) g\left(\boldsymbol{k}_g\right)\right) *^{-1} c\left(\boldsymbol{k}_g\right) \tag{8}$$

with $\boldsymbol{k}_g \in \mathbb{R}^{2 \times g}$ being new grid coordinates with the same ranges as $\boldsymbol{k}$. The weighting function $w_\omega(\boldsymbol{k})$ is calculated iteratively by $w_\omega(\boldsymbol{k}) = w_{\omega-1}(\boldsymbol{k})/(w_{\omega-1}(\boldsymbol{k}) * c(\boldsymbol{k})), w_0(\boldsymbol{k}) = 1, \omega \in \mathbb{N}$. With it, sampling coefficients are weighted by an area density compensation function to equalize the sample contribution to the new sampled coefficients.

The kernel $c(\boldsymbol{k})$ was analytically designed as described in [9] to optimize the reconstructed image in a circular field of view (FOV). It is given by

$$c(\boldsymbol{k}_{n,q}) = \left(\frac{J_1\left(\frac{m}{2}\pi\left|\boldsymbol{k}_{n,q}\right|\right)}{m\pi\left|\boldsymbol{k}_{n,q}\right|}\right)^2 \tag{9}$$

with J_1 denoting the Bessel function of first kind and order.

By convolution with the sampling function $g(\boldsymbol{k}_g)$ the data is sampled onto a new grid $\boldsymbol{k}_g$. In contrast to former time consuming propositions by Johnson et al. [9], we calculated all convolutions effectively using KD-trees [10].

Deapodization as inversion of the kernel convolution is realized in the image domain by dividing by the pseudoinverse of the kernel to remove aliased sidelobes of the image kernel. If the grid $\boldsymbol{k}_g$ is Cartesian, the reconstructed image $\tilde{\boldsymbol{x}}$ is gained by inverse discrete Fourier transform of $\tilde{\boldsymbol{y}}$.

2.6 Test setup

As the algorithm is built for arbitrary sampling trajectories, we exemplarily used periodically rotated overlapping parallel lines with enhanced reconstruction (PROPELLER) to evaluate the proposed algorithm. The k-space is divided into rectangular blades of the same size consisting of parallel lines. The blades are rotated around the k-space center in uniform angles. Pipe proposed the blades to contain m equidistant samples per line and $l = \frac{\pi m}{2N}$ lines for a circular FOV [11]. The motion was modeled as an autoregressive moving average process with maximal amplitude given to simulate a smooth patient motion for each motion parameter. It is sampled at N positions to extract each $\boldsymbol{\theta}_n$. Test images were the Shepp-Logan phantom in a FOV with a diameter of $m = 160$ and Brainweb simulations [12] in a FOV with a diameter of $m = 455$.

3 Results

Two reconstruction examples are given in Fig. 1. The Brainweb image was transformed by smaller motion and image details are reconstructed. The Shepp-Logan phantom was corrupted by large motion. No image, only motion artifacts are visible in the corrupted scene, but the image is reconstructed very well. Only a few gridding artifacts are visible. In Tab. 1, the mean percental improvement of the image quality measures peak signal-to-noise ratio (PSNR), structural similarity (SSIM), and mutual information (MI) calculated between the motion corrected and ground truth Shepp-Logan phantoms. The results for several numbers of partial measurements, maxima of translation and rotation are shown. High rates of improvement are reached. For Brainweb, similar results were gained.

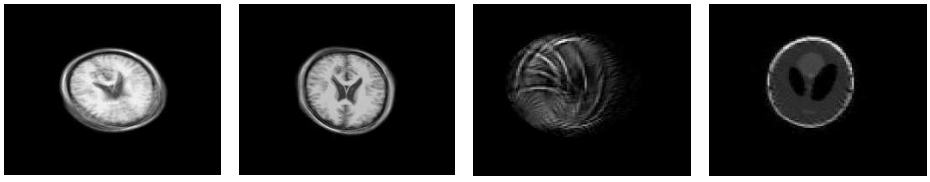

Fig. 1. Left to right: Brainweb image corrupted by motion with $\beta_{n,1}$, $\beta_{n,2} \leq 5, \alpha_n \leq \frac{\pi}{6}$, $N = 5$; motion compensated Brainweb image; Shepp-Logan phantom corrupted with $\beta_{n,1}, \beta_{n,2} \leq 30$, $\alpha_n \leq \frac{\pi}{6}$, $N = 8$; motion compensated Shepp-Logan phantom.

N	Trans	Rot	PSNR	SSIM	MI
5	5	$\pi/4$	4.35	2.87	8.50
8	10	$\pi/6$	6.73	4.97	23.99
5	30	$\pi/4$	6.73	4.82	28.08
6	30	$\pi/4$	8.08	5.32	30.06
6	30	$\pi/6$	9.74	5.36	23.28

Table 1. Percental improvement of the quality measures PSNR, SSIM, MI for N partial measurements with maximum translation (Trans) and maximum rotation angle (Rot) on the Shepp-Logan phantom.

4 Discussion

The motion compensation algorithm reaches reconstructions without motion artifacts and with a lot image details even for large motion. For small motion, image details are reconstructed even better. Only gridding artifacts remain in the images caused by low resolution. Overall, image quality measures are highly improved. A higher number of partial measurements comes with better motion compensation even if the number of samples per measurement gets smaller. With this blind motion compensation algorithm a new design for motion compensation for arbitrary sampling trajectories is given. Improvements could be reached by expansion to natural elastic motion and further reduction of gridding artifacts.

Acknowledgement. This work has been supported by the German Research Foundation under Grant No. ME 1170/11-1.

References

1. Pipe JG, Gibbs WN, Li Z, et al. Revised motion estimation algorithm for PROPELLER MRI. Magn Reson Med. 2014;72(2):430–437.
2. Möller A, Maaß M, Mertins A. Blind sparse motion MRI with linear subpixel interpolation. Proc BVM. 2015; p. 510–515.
3. Hormann K. Barycentric interpolation. Approximation Theory XIV: San Antonio. 2014; p. 197–218.
4. Aurenhammer F, Klein R, Lee DT. Voronoi Diagrams and Delaunay Triangulations. WORLD SCIENTIFIC; 2013.
5. Keiner J, Kunis S, Potts D. Using NFFT 3: a software library for various nonequispaced fast fourier transforms. ACM Trans Math Softw. 2009;36(4):19:1–19:30.
6. Parikh N, Boyd S. Proximal algorithms. Found Trends Optim. 2014;1(3):127–239.
7. Nocedal J, Wright SJ. Numerical Optimization. 2nd ed. New York: Springer; 2006.
8. Pipe JG, Menon P. Sampling density compensation in MRI: rationale and an iterative numerical solution. Magn Reson Med. 1999;41(1):179–186.
9. Johnson KO, Pipe JG. Convolution kernel design and efficient algorithm for sampling density correction. Magn Reson Med. 2009;61(2):439–447.
10. Bentley JL. Multidimensional binary search trees used for associative searching. Commun ACM. 1975;18(9):509–517.
11. Pipe JG. Motion correction with PROPELLER MRI: application to head motion and free-breathing cardiac imaging. Magn Reson Med. 1999;42(5):963–969.
12. Cocosco CA, Kollokian V, Kwan RKS, et al. BrainWeb: online interface to a 3D MRI simulated brain database. Neuroimage. 1997;5:425.